

# The active and passive populations of Extremely Red Objects.

Fabio Fontanot<sup>1,2</sup> & Pierluigi Monaco<sup>1,3</sup>

<sup>1</sup> *INAF-Osservatorio Astronomico, Via Tiepolo 11, I-34143 Trieste, Italy*

<sup>2</sup> *MPIA Max-Planck-Institute für Astronomie, Königstuhl 17, 69117 Heidelberg, Germany*

<sup>3</sup> *Dipartimento di Fisica, Università di Trieste, via Tiepolo 11, 34143 Trieste, Italy*

*email: fontanot@oats.inaf.it, monaco@oats.inaf.it*

Accepted ... Received ...

## ABSTRACT

The properties of galaxies with the reddest observed  $R - K$  colors (Extremely Red Objects, EROs), including their apparent division into passive and obscured active objects with roughly similar number densities, are a known challenge for models of galaxy formation. In this paper we produce mock catalogues generated by interfacing the predictions of the semi-analytical MORGANA model for the evolution of galaxies in a  $\Lambda$ CDM cosmology with the spectrophotometric + radiative transfer code GRASIL and Infrared (IR) template library to show that the model correctly reproduces number counts, redshift distributions and active fractions of  $R - K > 5$  sources. We test the robustness of our results against different dust attenuations and, most importantly, against the inclusion of TP-AGB stars in Simple Stellar Populations (SSPs) used to generate galaxy spectra, and find that the inclusion of TP-AGBs has a relevant effect, in that it allows to increase by a large factor the number of very red active objects at all color cuts. We find that though the most passive and the most obscured active galaxies have a higher probability of being selected as EROs, many EROs have intermediate properties and the population does not show bimodality in specific star formation rate (SSFR). We predict that deep observations in the Far-IR, from 100 to 500  $\mu\text{m}$ , are the most efficient way to constrain the SSFR of these objects; we give predictions for future *Herschel* observations, and show that a few objects will be detected in deep fields at best. Finally, we test whether a simple evolutionary sequence for the formation of  $z = 0$  massive galaxies, going through a sub-mm-bright phase and then a ERO phase, are typical in this galaxy formation model. We find that this sequence holds for  $\sim 25$  per cent of  $z = 0$  massive galaxies, while the model typically shows a more complex connection between sub-mm, ERO and massive galaxies.

**Key words:** galaxies: formation - galaxies: evolution

## 1 INTRODUCTION

The wealth of data coming from recent multiwavelength surveys has made it possible to study in detail distant galaxy populations from their UV-optical-Infrared broad-band spectral energy distributions (SED). Among the various categories that have been observationally defined by means of color selection techniques, the Extremely Red Objects (EROs) have attracted wide interest. Defined on the basis of their very red  $R - K$  color (in the Vega system  $R - K > 5$  at least), they were first addressed in the context of deep near-infrared surveys (Elston et al. 1988; McCarthy et al. 1992). Such red colors are expected to arise as a combination of an intrinsically red SED and a large  $K$ -correction at  $1 < z < 2$ . Then, EROs were regarded as natural counterparts of local elliptical galaxies (e.g. Cimatti et al. 2002a). Moreover, their relatively large  $K$ -band fluxes suggested high stellar masses, comparable with local ellipticals, leading to the interpretation of EROs as already assembled elliptical galaxies and the redshift range  $z > 2$  as their formation epoch. The correct prediction of such an early and efficient forma-

tion of massive galaxies at high redshift is a well known challenge for models of galaxy formation based on the CDM cosmology: in fact early implementations predicted lower space densities of EROs than observed (e.g., Firth et al. 2002; Smith et al. 2002).

On the other hand, it soon became evident that the same red  $R - K$  colors might be linked to a completely different class of objects such as the active (starburst) galaxies embedded in dust shells that cause high extinction of the SEDs (Cimatti et al. 2002a; Pozzetti & Mannucci 2000; Smail et al. 2002). Interestingly enough, the relative contribution to the total space density by the two sub-populations is similar, with a passive fraction of 48 per cent at  $K < 19.2$  (Kong et al. 2009, but a ratio between 30 and 70 per cent has been reported also by Cimatti et al. 2002a and Smail et al. 2002), and 58 per cent at  $K < 20.3$  (Miyazaki et al. 2003). However, splitting the observed ERO population in two is a difficult task. The cleanest way relies on high signal-to-noise spectroscopy, able to reveal either emission lines linked to ongoing star formation or the spectral breaks typical of aged stellar populations (see

e.g., Cimatti et al. 2002a). Alternatively, the presence of a starburst may be revealed by additional imaging in the far-infrared, where the absorbed light is reprocessed (Kong et al. 2009), or indirectly through the morphology of these objects (Stiavelli & Treu 2001; Cimatti et al. 2003). Presently, all these techniques can be successfully applied only to a small fraction of the overall population, typically limited to the brightest sources.

As mentioned above, the redshift distribution and the expected physical properties of the two ERO sub-populations have been a long-standing problem for theoretical models of galaxy formation (Cimatti et al. 2002a; Somerville et al. 2004). More recent models, based on improved treatment of baryonic physics (De Lucia et al. 2006; Bower et al. 2006; Menci et al. 2006; Monaco et al. 2007; Lagos et al. 2008), are able to give a better representation of the formation and assembly of massive galaxies at  $z < 3$ . Only a few of these models have been directly tested by comparing the predicted properties of EROs with data: in most cases a reasonable success in reproducing the abundance of passive EROs has been claimed, giving support to the interpretation of these objects as passive massive galaxies at  $z \sim 1 - 2$  that are the progenitors of local elliptical galaxy. At the same time, the same models do not produce a sufficient number of active EROs. More specifically, Nagamine et al. (2005) implemented sub-grid baryonic physics in both a Lagrangian and Eulerian code; they found the correct abundance of massive galaxies at  $z \sim 2$ , but could find almost no passive ERO, and in order to produce enough red galaxies they were forced to assume a dust attenuation as high as an equivalent  $E(B - V) = 0.4$  for the whole mock catalogue. Kang et al. (2006) correctly reproduced the space density of massive galaxies at  $z \sim 2$ , but underpredicted the number of very red galaxies, in particular of the active class. Menci et al. (2006) proposed a more successful model able to reproduce the color distribution of galaxies at  $z < 1$  and the space density of massive galaxies at  $1 < z < 2$  at the same time. This model is able to reproduce the ERO number counts and redshift distribution, but it predicts a relatively high fraction of passive objects ( $\sim 80$  per cent at  $K < 22$ ). More recently, Gonzalez-Perez et al. (2009) compared different implementations of the GALFORM model (Cole et al. 2000) to observational data of the ERO population. Their best fit model (i.e., Bower et al. 2006) produced the correct number of EROs, even when a very red cut (up to  $R - K > 7$ ) was used, but again the predicted ERO population was dominated by passive objects, with only a small fraction of active galaxies. On the other hand the model by Baugh (2006), which gives a good fit of the sub-mm galaxy population, was found to significantly underestimate ERO number counts.

A remarkable attempt to put quasars, bright sub-mm galaxies, EROs, and low- $z$  ellipticals into a unified scenario was proposed by Granato et al. (2004). In their model a typical low- $z$  elliptical forms the bulk of its mass in an intense obscured starburst phase at  $z \sim 2$ , when it is visible in the sub-mm band. In the galaxy nucleus, star formation triggers accretion onto a seed black hole; the end of the star formation phase is caused by feedback from the resulting quasar, able to wipe away the interstellar medium from the galaxy and quench star formation. After  $\sim 1$  Gyr the galaxy gets very red and becomes an ERO. It then evolves passively into a typical local elliptical galaxy.

The above mentioned papers have clarified the role of the ERO population as a powerful test for theoretical models of galaxy formation. These should reproduce both their global number and the diversity of their physical properties. A successful model would be helpful in investigating the relation of EROs with other observationally selected galaxy populations, in particular with the sub-mm

galaxies. Apparently, the most challenging requirement for published model is to produce a high fraction of active EROs, especially when deep samples are concerned. In principle, active EROs should be easy to produce in a hierarchical model of galaxy formation, because the redshift range where we observe them corresponds to the peak of the cosmic star formation rate density. Kong et al. (2006) and Nagamine et al. (2005) interpret the tension between their models and data as a sign of over-simplified recipes in treating baryonic physics or dust attenuations. Regarding the latter point, Fontanot et al. (2009a) showed that currently used recipes for dust attenuation, calibrated using low- $z$  samples, provide very scattered extinction values at  $z \sim 2$  and, more interestingly, do not match the predictions of the GRASIL code (Silva et al. 1998) that explicitly solves the equations of radiative transfer. Another important point is the contribution of the TP-AGB stars to the synthetic SEDs of model galaxies (see e.g. Maraston 2005), which is not included in the above mentioned models. It has been shown by Tonini et al. (2009a,b) that the inclusion of this extreme phase of stellar evolution has a strong impact on the expected photometry and colors of simulated galaxies at  $1 \lesssim z \lesssim 4$ , where intermediate-age stellar populations dominate the restframe  $K$ -band starlight. In the case of EROs, an increase of their number density is expected when TP-AGBs are included due to the reddening of rest-frame  $V - K$ . All these elements critically affect the modeling of galactic SEDs: they are therefore a primary concern for the interpretation of the physical ingredients of models.

In this paper we use the MORGANA model (Monaco et al. 2007, as updated in Lo Faro et al. 2009), interfaced with the GRASIL spectro-photometric + radiative transfer code Silva et al. (1998) and to Infrared (IR) template library (Rieke et al. 2009), to produce mock samples of EROs. We both use the *Padova* (Bertelli et al. 1994) and the Maraston (2005, M05 hereafter) library of SSPs. We find reasonable agreement with data in terms of number counts, redshift distribution and fraction of active objects, especially when M05 library is used (details on the effect of this modification on the whole galaxy population will be the subject of a forthcoming paper). This prompts us to use the model to investigate the physical properties of these object. We address whether there is a true active/passive bimodality of the ERO population and what is the connection between EROs, sub-mm galaxies and massive galaxies at  $z = 0$ . We finally give predictions of ERO properties for future surveys with the *Herschel* satellite.

This paper is organized as follows. In sec. 2 we recall the main feature of the theoretical models MORGANA and GRASIL. In sec. 3 we present our results: in sec. 3.1 we analyze the properties of the model ERO sample and in sec. 3.2 we discuss the connection between the ERO population, the sub-mm bright galaxies and the massive galaxies at  $z = 0$ . Finally in sec. 4 we give our conclusions. Throughout the paper we assume magnitudes are in the Vega system (unless otherwise stated), and a cosmological model consistent with WMAP3 results ( $\Omega_0 = 0.24$ ,  $\Omega_\Lambda = 0.76$ ,  $h = 0.72$ ,  $\sigma_8 = 0.8$ ,  $n_{sp} = 0.96$ , Komatsu et al. 2009).

## 2 MODEL

We use the semi-analytical MOdel for the Rise of GALaxies aNd AGNs (MORGANA), originally presented in Monaco et al. (2007), and updated in Lo Faro et al. (2009), where it was optimized for the WMAP3  $\Lambda$ CDM cosmology used in this paper, *Padova* SSP library and a Chabrier (2003) stellar Initial Mass Function (IMF). All details are reported in the former paper, while a brief outline is given

in the latter; we refer to them for a description of the model. The only new extension we present in this paper is the use of M05 library as an alternative to the *Padova* ones. The predictions of MORGANA were compared with a number of observations in a series of papers (Fontanot et al. 2006, 2007, 2009b). In those papers the model was calibrated to reproduce the local stellar mass function and the star formation rate density as a function of redshift, while some parameters (especially those regulating accretion onto central black holes) were fixed by requiring a good fit of AGN luminosity functions. Among the most interesting successes of the model, MORGANA is able to correctly reproduce, with the same combination of parameters, (i) the evolution of the AGN population and in particular the optical and X-ray luminosity functions; (ii) the redshift distribution and luminosity functions of *K*-selected samples in the redshift range  $0 < z < 3$ ; (iii) the number counts of  $850\mu\text{m}$ -selected sources assuming a conservative Salpeter or Chabrier IMF. Moreover, the progressive build-up of bright Lyman-break galaxies at  $z \gtrsim 4$  is recovered after the optimization of dust attenuation parameters that have a dramatic influence on rest-frame UV radiation.

*K*-band and sub-mm counts of MORGANA galaxies were shown by Fontanot et al. (2007) for the original version of the model. With the change of cosmology, IMF and the improvements given in Lo Faro et al. (2009), *K*-band number counts are very similar to those presented in Fontanot et al. (2009b), with a better fit at  $K \sim 18$ , roughly corresponding to the knee of the local luminosity function. The agreement of the redshift distribution of  $K < 20$  galaxies with observations shows a slight but appreciable improvement. Though the stellar mass function is well recovered at high masses with the improved model (Fontanot et al. 2009b), we still produce an excess of bright galaxies in the *K*-band local luminosity function (for  $K < -25.5$ , amounting to  $\sim 1$  dex at  $M_K = -26.5$ ). This is due to the too high specific star formation rate of local massive galaxies (see below), which results in mass-to-light ratios  $M_*/L_K \sim 0.5M_\odot/L_\odot$ , to be compared, e.g., with the value of 0.75 assumed by Cole et al. (2001) to convert the local *K*-band luminosity function into a stellar mass function (see Fontanot et al. 2007 for a complete discussion of this issue). Sub-mm counts are depressed by a factor of 0.5 dex when passing from Salpeter to Chabrier IMF, while their redshift distribution does not change appreciably: this implies that in the new model sub-mm number counts are consistent with data up to a flux of 3 mJy, while they are underpredicted at brighter fluxes.

Previous papers have found a number of points of severe tension between model and data, some of which are also present for most similar models.

(i) The colors of model massive galaxies at low redshift are too blue (Kimm et al. 2009): this is a peculiar problem of MORGANA and is mainly due to the modeling of AGN feedback: because star formation is required to trigger black hole accretion, an efficient AGN feedback requires some small amount of star formation to take place, and this makes massive galaxies bluer than observed.

(ii) The color distribution of low-*z* satellite galaxies is not correctly reproduced, with the fraction of red satellites outnumbering the corresponding blue fraction (Weinmann et al. 2006). This is directly related to “strangulation”, i.e. the assumption that satellites are stripped of all their hot gas when they infall on a larger group. Kimm et al. (2009) recently showed that this problem is common to most semi-analytic models of galaxy formation.

(iii) The so-called “downsizing” trend in galaxy formation (e.g. more massive galaxies forming on a shorter timescale and at higher redshift with respect to lower mass counterparts) is not fully re-

covered. The tension between model predictions and observations is significant for low-to-intermediate stellar mass galaxies ( $M_* < 10^{11}M_\odot$ ): they form too efficiently at high redshift (Lo Faro et al. 2009, see also) and are too passive at later time, so that the model overpredicts their observed stellar mass function at  $z > 1$ . As a result such small galaxies are predicted to host too old stellar population at  $z = 0$ . Fontanot et al. (2009b) showed that this behavior is common to most published models based on  $\Lambda$ CDM (i.e. Wang et al. 2008; Somerville et al. 2008).

(iv) The number of massive galaxies at  $z > 3$  is underpredicted by MORGANA: despite the evolution of the *K*-band luminosity function is reasonably reproduced by the model up to  $z \sim 2$  (Fontanot et al. 2007), Cirasuolo et al. (2007, 2008) showed that at higher redshifts the bright end is systematically underpredicted. A similar effect is seen in the evolution of the stellar mass function (Fontanot et al. 2009b). This tension is expected to weaken when TP-AGB stars are included in the population synthesis model used to generate the SEDs (Tonini et al. 2009b), though Marchesini et al. (2009) find that this is not sufficient to remove the discrepancy.

(v) Specific star formation rates of active galaxies at  $z \sim 2$  in MORGANA galaxies are higher than those of other models, but they may still be a factor of  $\sim 3$  lower than observed ones (Santini et al. 2009; Fontanot et al. 2009b), though this difference may well be due to systematics in star formation rate estimators.

(vi) Higher specific star formation rates are clearly the key for the success of MORGANA in reproducing the elusive sub-mm counts, but the redshift distribution of the most luminous sub-mm sources peaks at lower redshift than observed by Chapman et al. (2005). This discrepancy is clearly connected with the lack of downsizing in the model: massive starbursts should take place earlier than average, not later as in our model.

All these issues can influence our results on the ERO population; for instance, a population of strangulated satellites could artificially boost the number of EROs, while residual star formation in massive galaxies could depress it. We will keep in mind all these discrepancies when interpreting our results.

## 2.1 Generation of mock catalogues

We generate our main mock catalogue using a PINOCCHIO (Monaco et al. 2002) simulation of a  $200Mpc$  comoving box, sampled with  $1000^3$  particles. The particle mass is then  $\sim 10^9M_\odot$  and the smallest halo we consider contains 50 particles, for a mass of  $5.1 \times 10^{10}M_\odot$ . The typical stellar mass of the central galaxy contained in the smallest DM halo at  $z = 0$  is  $\sim 5 \times 10^8M_\odot$ . The same sampling strategy to generate deep fields as in Fontanot et al. (2007) is adopted here, with the only difference that, in order to have a sufficient number of EROs, all merger trees in the box are used ( $w_{\text{tree}} = 1$  in the original notation, see the original paper for more details on sampling strategy and catalogue generation). The final reference mock catalogue consists in  $\sim 240000$  model galaxies, covering a redshift range  $0 < z < 8$ .

MORGANA provides predictions on galaxies in terms of physical, non observable quantities. We then interface MORGANA with the spectro-photometric + radiative transfer code GRASIL (Silva et al. 1998). This code computes the synthetic UV-to-radio SEDs of galaxies from the known star formation history, cold gas mass, cold gas metal mass and size, separately provided for a bulge and a disc component. Further assumptions are made on bulge profile, vertical width of the disc, dust distribution in molecular clouds and diffuse gas. Stars are assumed to be born within the optically

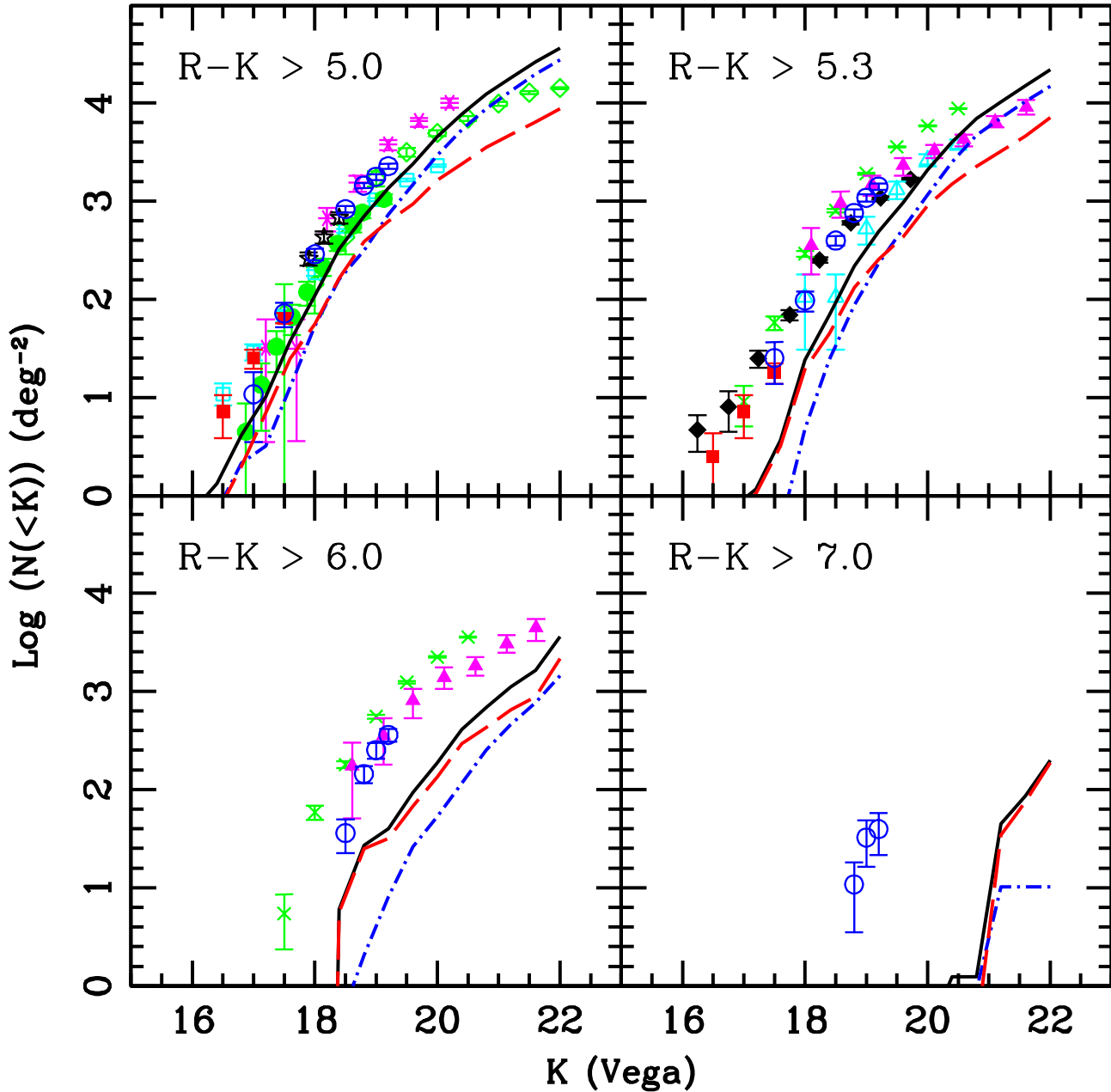


**Figure 1.** ERO cumulative number counts in the reference model for four  $R - K$  (Vega) color cuts, as given in the panels. Observational datapoints are taken from Daddi et al. (2000, blue empty circles), Smail et al. (2002, cyan empty triangles), Smith et al. (2002, magenta filled triangles), Roche et al. (2003, black empty diamonds), Miyazaki et al. (2003, magenta asterisks), Väisänen & Johansson (2004, red filled squares), Brown et al. (2005, black stars), Simpson et al. (2006, green crosses), Kong et al. (2006, green filled circles), Lawrence et al. (2007, cyan empty squares), Conselice et al. (2008, black filled diamonds). Solid black lines refer to the prediction for the whole ERO population, red dashed and blue dot-dashed lines refer to the passive and active classes respectively.

thick molecular clouds and to gradually escape from them as they get older. This gives rise to an age-selective extinction, with the youngest and most luminous stars suffering larger dust extinction than older ones. The radiative transfer of starlight through dust is computed assuming an axisymmetric bulge-disc system, yielding the emerging SED. Some of the parameters needed by GRASIL are not directly provided by MORGANA. We fix their values as in Fontanot et al. (2007), where a choice was made which is good for

the average galaxy population: in particular we use an escape time-scale of young stars for the parent molecular clouds equal to  $10^7$  yr and a 0.5 fraction of cold gas mass in the form of molecular clouds. These values differ from the choice done in Lo Faro et al. (2009), which was optimized for high- $z$  Lyman-break galaxies: escape time equal to  $0.3 \times 10^7$  yr and a 0.95 molecular fraction. As shown by Silva et al. (2005), the final fraction of active EROs in their model depends strongly on these unconstrained parameters: this is espe-

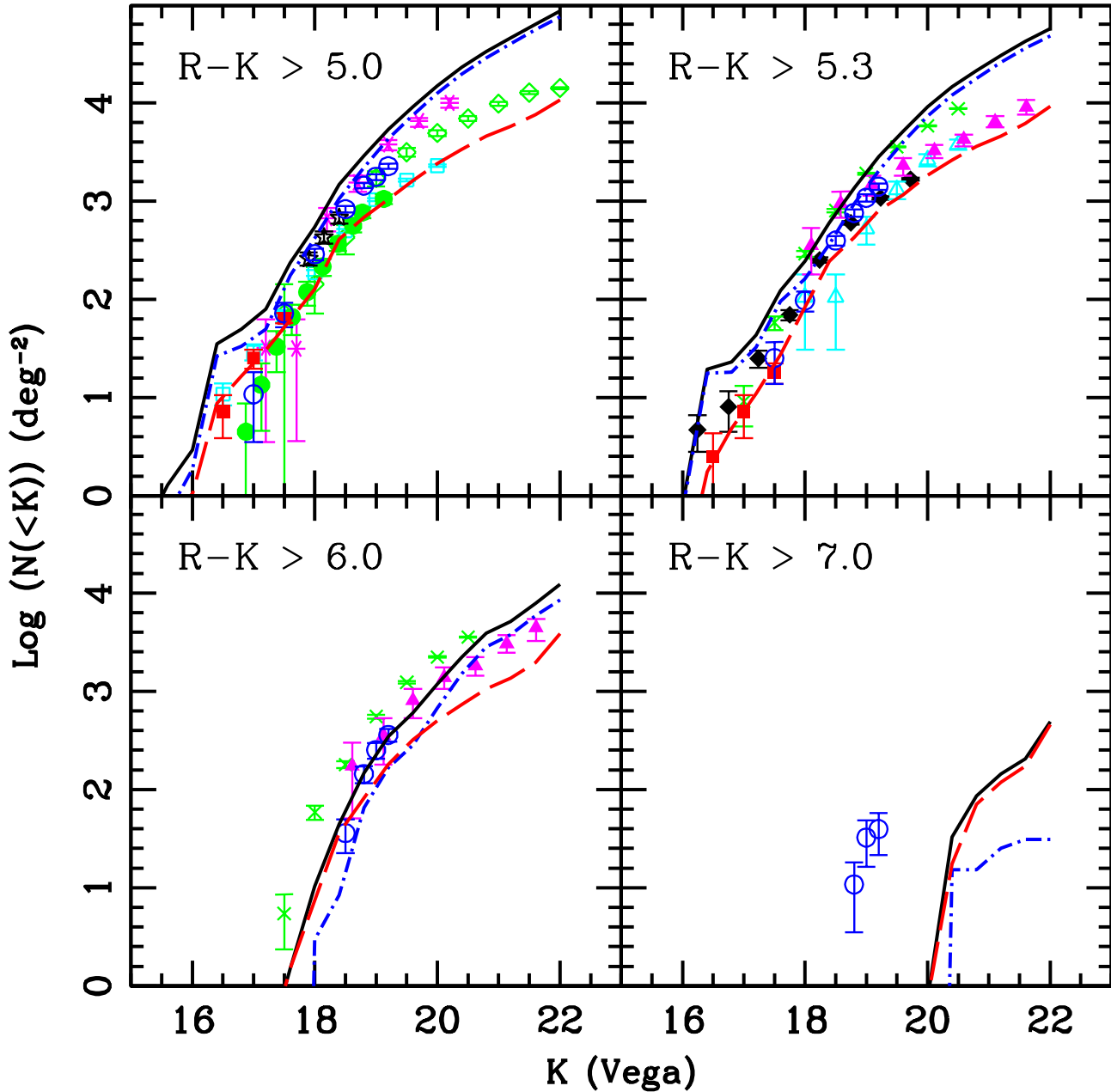


Figure 2. ERO cumulative number counts in the model using M05 SSP library for four  $R - K$  (Vega) color cuts. Symbols and lines are as in figure 1.

cially true for the objects at  $z > 1$ , which require a detailed computation of the highly uncertain dust obscuration in the restframe UV. They reported that obscuration is especially sensitive to the assumed molecular fraction. Because our aim in this paper is to test the predictions of already published versions of the model and not to find the best-fit parameters for this specific observables, we decided to use the parameters of Fontanot et al. (2007), and test how results change using the high molecular fraction of Lo Faro et al. (2009). Apparent magnitudes are computed by adding a fiducial 0.1 mag random Gaussian error. Number counts and redshift distributions are then constructed as in Fontanot et al. (2007). It is worth stressing that our reference MORGANA+GRASIL model is

calibrated using the *Padova* SSP library. Here, we also produce a catalogue using the M05 SSP library (which adopts a Kroupa et al. (1993) IMF - we neglect the small differences with the Chabrier IMF), to check the effect of the inclusion of the TP-AGBs on the ERO statistics.

Given the low space density of the ERO population, a higher sampling of model galaxies is required with respect to the mock catalogues defined in Fontanot et al. (2007). In order to speed up computations (see Fontanot et al. 2007 for a general discussion about the time requirements of the MORGANA+GRASIL algorithm), we modify our standard approach as follows. For each model galaxy we compute the UV-to-Near-IR SED with GRASIL,



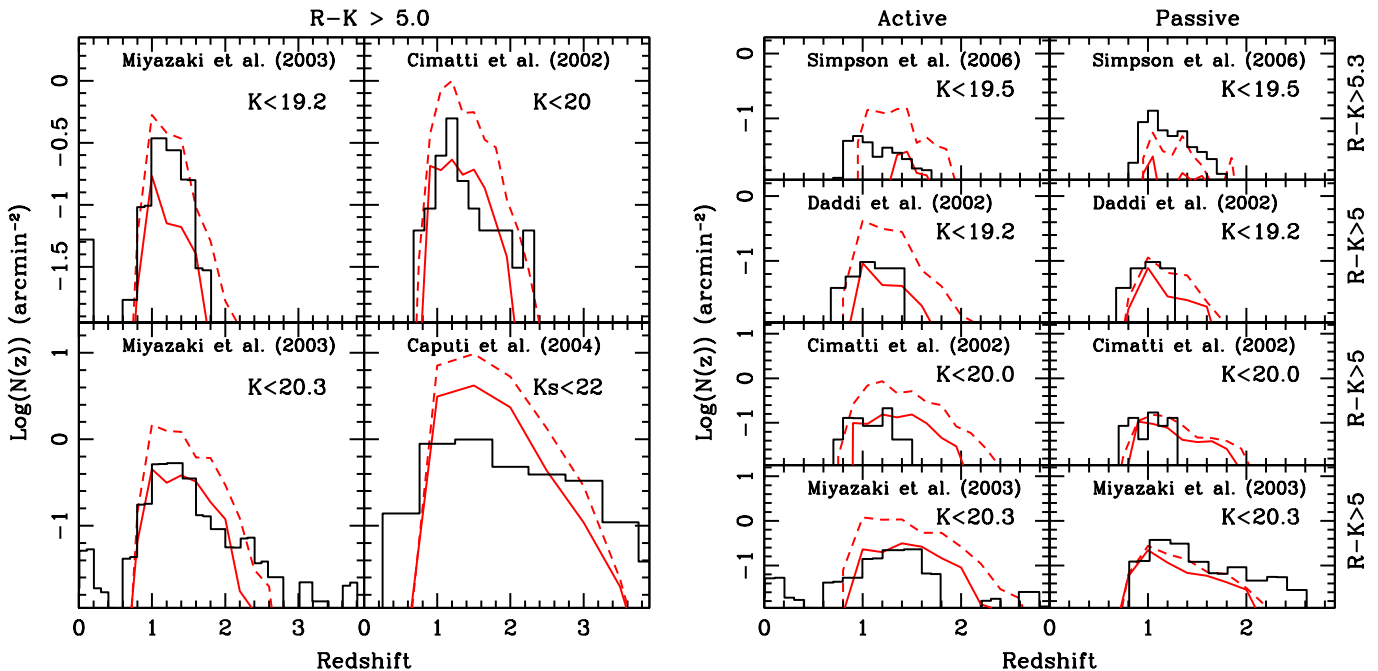


**Figure 3.** Left: predicted and observed ERO redshift distributions at the flux limits given in the panels. Data are from Cimatti et al. (2002b, spectroscopic completeness 67%), Miyazaki et al. (2003, photometric redshifts), Caputi et al. (2004, photometric redshifts). The continuous and dashed lines refer to the model predictions with *Padova* and M05 SSP library, normalized to the same area of the corresponding surveys. Right: observed and predicted ERO redshift distributions splitted into active and passive populations. Data taken from Daddi et al. (2002, spectroscopic redshifts), Cimatti et al. (2002b), Miyazaki et al. (2003) and Simpson et al. (2006, photometric redshifts).

including dust attenuation but excluding the computation of the Far-IR emission due to heated dust, which is by far the most time-consuming step. With this choice we are then able to generate the synthetic SEDs in a few seconds instead of  $\sim 5 - 10$  min. We then compute the total absorbed starlight and we use it to select an appropriate IR template from the Rieke et al. (2009) library. We renormalize the chosen template to the total absorbed starlight and use it to model IR emission, which is significant for fluxes at  $\lambda > 3\mu\text{m}$ . As shown in Fontanot et al. (2010), this procedure provides an estimate for the SED which is however, for high-redshift galaxies, biased low by  $\sim 0.2$  dex at high sub-mm luminosities but is correct on average at fluxes of  $\lesssim 1$  mJy, with respect to GRASIL code. As a cross check, we apply a full GRASIL calculation to a much smaller mock catalogue of  $\sim 32000$  galaxies and compare the resulting number counts and redshift distribution with those based on IR templates. No significant differences were found at  $\lambda < 850\mu\text{m}$ . The normalization of sub-mm number counts is correctly reproduced at fluxes  $f_{850\mu\text{m}} \sim 0.5$  mJy; at brighter fluxes the counts are underpredicted by a factor of 4 at  $f_{850\mu\text{m}} \sim 3$  mJy, due to the low biasing of this procedure with respect to the predictions of the full GRASIL calculations, while at fainter fluxes ( $> 0.1$  mJy) they are overpredicted by a similar amount.

### 3 RESULTS

In fig. 1 we compare the predicted ERO cumulative number counts (black line) with available data (Daddi et al. 2000; Smith et al. 2002; Smail et al. 2002; Roche et al. 2003; Väisänen & Johansson 2004; Brown et al. 2005; Kong et al. 2006; Simpson et al. 2006; Lawrence et al. 2007; Conselice et al. 2008), for color cuts ( $R - K$ )  $> 5.0, 5.3, 6.0$  and  $7.0$ . We first consider the predictions of

our reference model: for the first color cut, the agreement is good down to  $K \sim 20$ , where the model starts to overpredict number counts. This behavior is very similar to that of the total sample (figure 2 of Fontanot et al. 2007). We stress that this level of agreement is obtained, with no parameter tuning, from the same model used in Fontanot et al. (2009b) and Lo Faro et al. (2009). The agreement worsen at redder colors: the brightest sources at  $(R - K) > 5.3$  are underpredicted by an order of magnitude, lowering to a factor of 3 at  $K \sim 18$ ; we find an overall underestimate by an order of magnitude for  $R - K > 6$  and a much more severe one for  $R - K > 7$ .

We then split the whole ERO population into active and passive subsamples using the instantaneous specific star formation,  $\text{SSFR} = \text{SFR}/M_*$ . As a threshold between the two populations we assume the same criterion as in Brinchmann et al. (2004,  $\text{SSFR} = 10^{-11} \text{yr}^{-1}$ ) at all redshifts: at the depth of  $K = 22$  and for  $R - K > 5.0$  we classify  $\sim 68$  and  $\sim 32$  per cent of model EROs as active and passive respectively. At  $K < 20.3$  the relative fractions of active and passive EROs become  $\sim 62$  and  $\sim 38$  per cent to be compared with the results of Miyazaki et al. (2003, , 42 and 58 per cent respectively), while at  $K < 19.2$  the fractions are  $\sim 53$  and  $\sim 47$ , consistent with the results of Cimatti et al. (2002a, both  $50 \pm 20$  per cent). Finally at  $R - K > 5.3$  and  $K < 20.5$  our model predicts a relative fraction of 56% active EROs, to be compared with the results of Smail et al. (2002), who found an active fraction ranging from a lower limits of 30% up to an upper limit of 60%. Figure 1 gives the predicted cumulative number counts for the two classes of EROs; for the first color cut passive EROs (red dashed line in the figure) are more numerous at bright fluxes, active ones (blue dot-dashed line) start to dominate at  $K > 18.5$ .

To test the stability of our results against different SSP libraries and models of dust attenuation we repeat the analysis using

different assumptions for these ingredients. We create three mock catalogues by interfacing the same MORGANA realization with the following modifications to our standard GRASIL setup:

(i) we consider a higher molecular fraction (0.95) and a lower escape time for stars (3 Myr) in active galaxies, as used by Lo Faro et al. (2009) to reproduce the properties of bright Lyman Break Galaxies;

(ii) we model dust extinction using the prescription proposed by De Lucia & Blaizot (2007), which combines their fitting formula for the optical depth in the  $V$ -band with a slab geometry and a composite age-dependent attenuation law (i.e. assuming a Milky Way extinction curve for the diffuse “cirrus” dust and the Charlot & Fall 2000 power-law attenuation law for the younger stars).

(iii) we use the M05 SSP library in place of the *Padova* one.

Our results show that changing dust parameters or the modeling of extinction has only a marginal effect on the shape and normalization of the number counts. Increasing the fraction of cold gas in the molecular phase depresses the counts of active objects by 0.3 dex at  $K \sim 20$ , while the passive population is unaffected. A similar decrease (0.1 dex) is observed when using the analytical attenuation law of De Lucia & Blaizot (2007); in this case only  $\sim 49$  per cent of the original EROs are selected, while an additional  $\sim 21$  per cent (with respect to the original number) is added to the sample. In both tests on dust attenuation, all the removed objects, as well as the new inclusions, belong to the active subsample. Since the intrinsic synthetic SEDs do not change in these tests, the differences in the colors of model galaxies arise from the different attenuation laws. Indeed it has been shown by Fontanot et al. (2009a) that De Lucia & Blaizot’s analytical attenuation law is a good approximation of the mean attenuation law in a MORGANA+GRASIL realization, but the scatter is large. At the same time, a different choice of dust parameters is able to change both the mean and scatter of the distribution.

On the other hand, we find that using M05 SSP library gives the strongest effect on ERO number counts, causing a relevant increase of EROs at all color cuts; the active population becomes dominant at all fluxes. In this case the change in the colors of model galaxies is mainly driven by a change in the intrinsic shape of their synthetic SEDs. In fig. 2 we show the integral number counts in this last model:  $R - K > 5.0$  counts are slightly overpredicted at all magnitudes, while the  $R - K > 5.3$  bright counts now agree with observations; more interestingly the  $R - K > 6.0$  are now in excellent agreement with observations, while the  $R - K > 7.0$  sources are still under represented in the model. Using a higher molecular fraction or De Lucia & Blaizot’s analytical attenuation law in conjunction with the M05 SSP library allows a further (marginal) improvement of model predictions with data.

In fig. 3 we compare the redshift distribution of model EROs with available data. In the left panels we consider the redshift distribution of the global population (Cimatti et al. 2002b; Miyazaki et al. 2003; Caputi et al. 2004) different  $K$ -band magnitude limits. For our standard model (solid line), the agreement is good in the probed range: EROs are mostly present in the redshift range  $[0.8, 2]$  (mean redshift 1.34 at  $K < 20$ ), with a sharp low-redshift cutoff which is well reproduced and a high-redshift tail which is under-represented by the model. Regarding the normalization, we notice again some excess at fainter magnitudes and some possible underestimate at  $K < 19.2$ , which is however not confirmed by other surveys shown in figure 1. When the sample is split into active and passive populations, we see a marginal trend of passive galaxies peaking at slightly lower redshift, which our

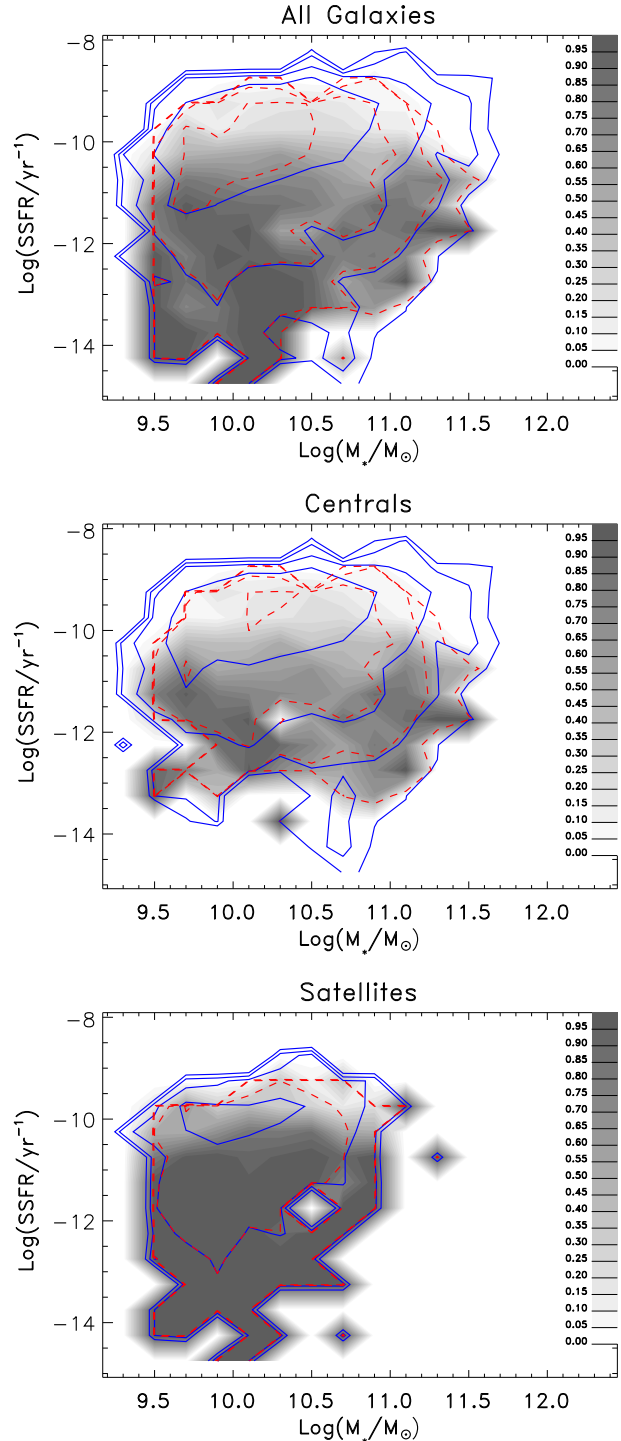


**Figure 4.** Upper panel: 2D probability density of model galaxies in the  $M_*$  – SSFR space. Blue continuous lines are iso-density contours spaced by factors of 10 in density, and are relative to the control sample of all galaxies with  $K < 22$  and in the redshift range  $z = [1, 2]$ . Dashed red lines give the same quantity for the ERO population. Gray-scale contours give the fraction of EROs with respect to the control sample in the same  $M_*$ –SSFR bin, using the scale given on the right. The mid and lower panels report the same quantity for central and satellite galaxies respectively.

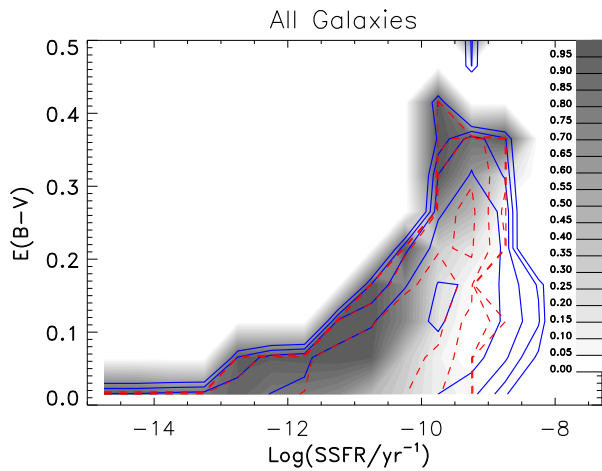


**Figure 5.** 2D probability density of model galaxies in the SSFR –  $E(B-V)$  space. Symbols are as in fig. 4.

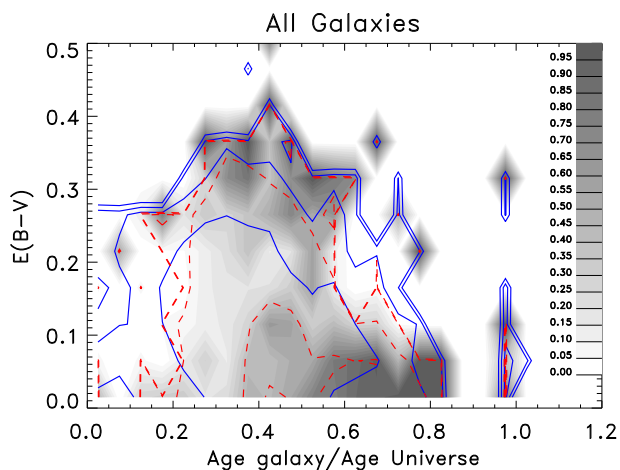


**Figure 6.** 2D probability density of model galaxies in the space defined by mass weighted age, divided by the age of the Universe at the redshift of observation, and  $E(B-V)$ . Symbols are as in fig. 4.

model roughly reproduces (mean redshift 1.27 and 1.13 at a depth of  $K = 20$  for the active and passive populations respectively); moreover, from the richer Miyazaki et al. (2003) sample we see that the under-reproduction of the high-redshift tail is mostly due to passive galaxies, while active EROs are possibly over-represented. The modified models with different dust parameters or analytical attenuation law predicts redshift distributions that are almost undistinguishable from the standard model. The model with the M05 SSPs predicts similar redshift distribution (mean redshift 1.34, 1.25, 1.15 at  $K < 20$  for the total, active and passive populations respectively), but higher number densities (dashed lines). This is especially relevant for the active subpopulation. We also show the redshift distribution for the redder cut  $R - K > 5.3$  (Simpson et al. 2006) and we find that they preferentially select EROs at higher redshift; our model with M05 library reproduces this trend.

These tests show clearly that, among the three changes in SED modeling that we tested, the inclusion of TP-AGBs has a strongest effect on the number counts, and in particular, on the active subpopulation. The detailed analysis of the effects of this inclusion on

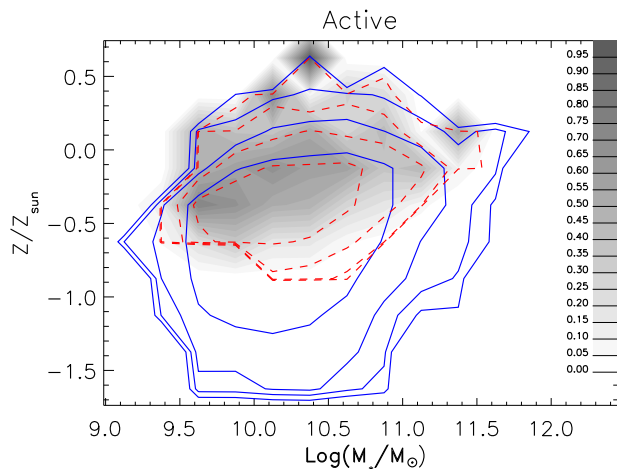
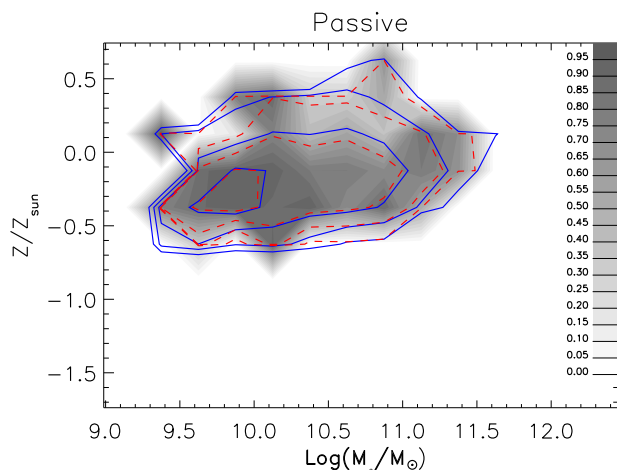
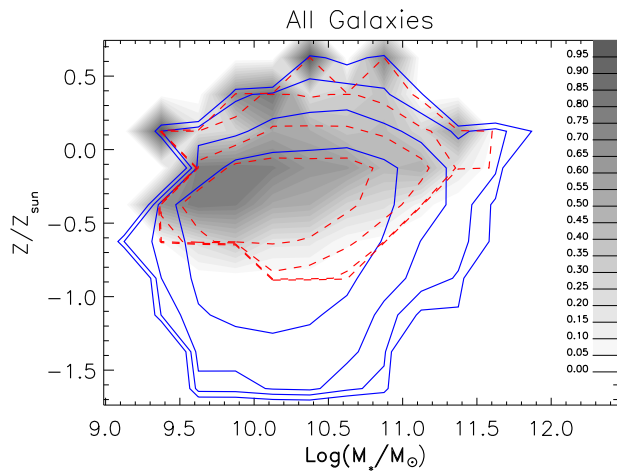


**Figure 7.** Upper panel: 2D probability density of model galaxies in the  $M_* - Z_*$  space. Symbols are as in fig. 4. The mid and lower panels report the same quantity for passive and active galaxies respectively.

the whole galaxy population and its redshift evolution is clearly beyond the aim of this paper and we leave it to future work. For this reason, and in order to allow a direct comparison with the previously published results for the same model, we decided to discuss the physical properties of EROs only for the reference model with Padova SSPs, which is able to reasonably reproduce counts and redshift distributions of the  $R - K > 5.0$  sources, even when we



split the population into active and passive subsamples. We checked that the results presented in the rest of this paper do not change significantly when the model including M05 SSPs is used.

Summing up, the three main points of disagreement of our reference model with data are: (i) an excess of faint EROs, (ii) an underestimate of EROs at high color cuts, (iii) an underestimate of high-redshift passive EROs. These discrepancies are consequences of the known problems of the model: the excess of small galaxies at  $z \sim 1$  that affects most galaxy formation models reflects in the excess of faint EROs, while because the reddest galaxies are higher-redshift sources, points (ii) and (iii) are usually related with the dearth of high-redshift massive galaxies in MORGANA (Fontanot et al. 2007). It is worth stressing that when TP-AGB stars are taken into account, the tension at points (ii) and (iii) is considerably reduced (but not completely solved): this is an hint of the relevance of the detailed inclusion of this stellar evolutionary phase in the algorithms for the estimate of stellar masses (Maraston et al. 2006).

### 3.1 Properties of the ERO populations.

The good level of agreement of model EROs with observations at  $R - K > 5$ , especially in terms of fraction of active and passive objects, encourages us to use the model to get insight on the properties of the two ERO populations and on their relation with sub-mm galaxies and local massive galaxies. To this aim we consider the predicted physical properties of the  $K < 22$ ,  $R - K > 5$ ,  $1 < z < 2$  ERO galaxies, and compare them with a control sample containing all galaxies with  $K < 22$  and in the same redshift range. In the following we will consider only predictions relative to our reference model, but we checked that the inclusion of any of the modifications we discussed in the previous section does not affect our conclusions. In figure 4 we show the 2D probability density of ERO (red dashed lines) and control sources (blue continuous lines) in the stellar mass – SSFR space. The gray-scale contours give the fraction of galaxies in that stellar mass and SSFR bin that meet the selection criterion. Overall, EROs do not populate a special region in this space with respect to the global population at similar redshift and, consistently with Gonzalez-Perez et al. (2009), they do not show a bimodal distribution of either passive or active galaxies. Passive galaxies show a higher probability of satisfying the ERO selection; the most active galaxies are typically selected out.

A crucial point of galaxy formation models is the different behavior of central and satellite galaxies; in particular, strangulation of satellites may artificially boost the number of EROs. To deepen this point we separately show the ERO and control distributions of centrals and satellites in the  $M_* - \text{SSFR}$  space, in the two upper panels of fig. 4. As expected, satellites are more passive than centrals and centrals are more massive than satellites, and this is true both for the ERO and for the control samples, but the populations of active and passive EROs are present in both sub-samples, and the differences between the distributions in the two cases are not so strong. We cross-checked this result by comparing integral number counts of ERO central galaxies with all EROs, finding only a small difference. In particular, the faint end of the number counts is reduced by  $< 0.3$  dex, while the bright end is unaffected. This is due to the fact that the population of  $M_* > 10^{10} M_\odot$  galaxies is dominated by centrals. We conclude that the statistics of model EROs is unaffected by artificial strangulation of satellites.

The absence of a clear bimodality in the distribution of ERO SSFR is at variance with early ideas on the nature of these objects as either massive passive galaxies or heavily obscured starbursts.

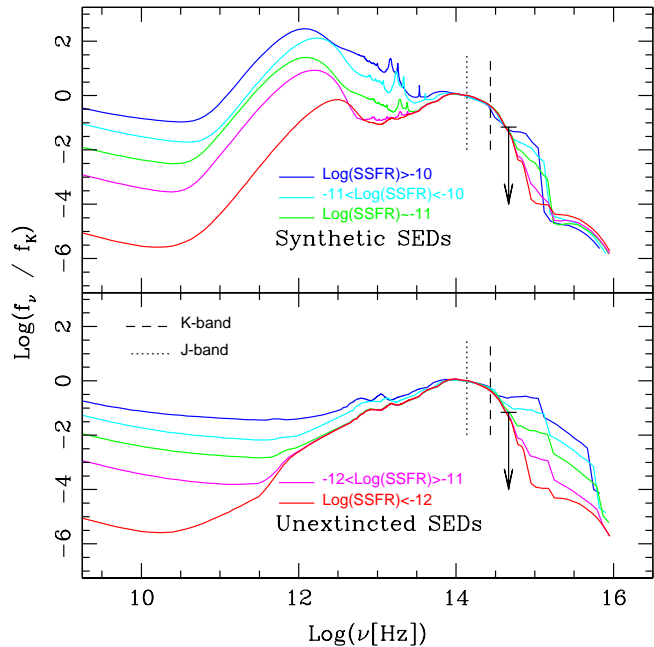


**Figure 8.** Comparison between typical SEDs for different activity levels. All SEDs have been normalized to the K-band flux. Upper panel show the GRASIL synthetic SED, while lower panel show the corresponding intrinsic starlight emission. Blue and red lines refer to very active ( $\text{SSFR} > 10^{-10} \text{yr}^{-1}$ ) and very passive ( $\text{SSFR} < 10^{-14} \text{yr}^{-1}$ ) objects in the mock catalogue. Cyan, green and magenta lines represents typical SEDs for EROs with  $10^{-10} \text{yr}^{-1} < \text{SSFR} < 10^{-11} \text{yr}^{-1}$ ,  $\text{SSFR} \sim 10^{-11} \text{yr}^{-1}$ ,  $10^{-11} \text{yr}^{-1} < \text{SSFR} < 10^{-12} \text{yr}^{-1}$  respectively.

To further investigate whether a bimodality is present in the model ERO population, we define the color excess  $E(B - V)$  as:

$$E(B - V) = (B - V) - (B - V)^0 \quad (1)$$

where  $(B - V)^0$  represents the intrinsic color computed on the rest-frame synthetic SEDs before dust extinction, while  $(B - V)$  is computed after dust extinction. In fig. 5 we show the 2D probability density of control and ERO galaxies in the  $\text{SSFR} - E(B - V)$  color space. Contours are as in figure 4. Also in this space, active and passive EROs do not populate separate regions, but they define a unimodal distribution, very similar to that of the overall galaxy population. Passive galaxies are characterized by low attenuations as expected, and color excesses range up to a maximum of  $\sim 0.4$  for active galaxies. EROs do not populate the region of strongly star-forming galaxies with  $E(B - V) < 0.2$ . We find a clear bimodality when we consider the distribution of the fraction of galaxies with very red colors, which shows two broad peaks for passive galaxies with  $E(B - V) < 0.2$  and very active ones,  $\text{SSFR} > 10^{-10} \text{yr}^{-1}$  and  $E(B - V) > 0.2$ . This result does not give support to the assumption of high attenuations for active EROs made by Nagamine et al. (2005). In fig. 6 we show the location of control and ERO galaxies in the space defined by the mass-weighted ages of the stellar populations, normalized to the age of the Universe at the observation redshift, and  $E(B - V)$ . EROs tend to avoid the region at low age and attenuation, and again their fraction show a bimodal trend in  $E(B - V)$ , but no bimodality is visible in the overall distribution. Finally, we show in figure 7 the location of EROs in the stellar mass-metallicity relation. EROs tend to selectively populate the high metallicity region. This is the result

of the combination of two effects, as can be seen from the smaller panels. Passive galaxies populate only the high metallicity region, as expected from evolved stellar populations. The control population of active galaxies shows a larger spread, but only sources with high metallicity reach the high levels of obscuration required to be selected as an ERO.

The distinction between active and passive EROs is an observational crucial point. From figure 4 we see that SSFR values for EROs have a broad and unimodal distribution, so that moving the cut around the assumed value of  $10^{-11} \text{ yr}^{-1}$  will not change much the relative fractions of the two classes. To better illustrate the continuity of EROs along the SSFR parameter, in fig. 8 we show five typical SEDs (in the observed frame) for EROs in our mock catalogue with various SSFR values. SEDs are normalized at the  $K$ -band wavelength, in order to highlight the differences in SED shapes. We choose two extreme examples of active and passive galaxies ( $\text{SSFR} > 10^{-10} \text{ yr}^{-1}$  and  $\text{SSFR} < 10^{-14} \text{ yr}^{-1}$ ) and three objects with intermediate SSFR; in particular the green line represents an object with SSFR close to the activity threshold, while the cyan and magenta lines refer to objects with activity respectively higher and lower than the threshold by less than a factor of 10.  $K$  and  $J$  central wavelengths are shown by dotted and dashed lines, while at central  $R$ -band wavelength we report the upper limit for ERO selection. This comparison highlights the continually varying properties of SEDs along the SSFR sequence, with no clear difference in the predicted spectral properties in the Near-IR. Larger differences are present at longer wavelengths ( $\lambda > 10 \mu\text{m}$ ), so observations in the Mid-IR and, especially, in the Far-IR can provide a clear distinction between active and passive EROs.

Such observations can in principle be carried out by the *Herschel* Far-IR space telescope. We show in fig. 9 the predicted relation between the SSFR of EROs and the ratio between  $K$ -band and monochromatic fluxes in four bandpasses covered by the instruments on board *Herschel*, in our smaller mock catalogue where IR fluxes are computed using full GRASIL calculations. All four colors show a clear correlation with SSFR; we find much weaker trends for fluxes at shorter wavelengths, as those currently probed by the *Spitzer* space telescope. These correlations are stronger at high levels of specific star formation, while passive galaxies split into two distinct sequences. This splitting relates to the modeling of star formation in bulges or discs: the upper sequence is dominated by galaxies with *bulge-to-total* mass ratios  $> 0.6$  (as in Fontanot et al. 2009a), denoted by red crosses while cyan squares correspond to disc-dominated galaxies. We checked that this splitting is mainly due to the presence of a population of passive and high-metallicity discs, that give rise to the lower branch. Getting back to active galaxies, it is evident that a Far-IR follow-up of the already-known EROs would be of great importance in order to have a better understanding of the properties of these objects, and in particular on their star formation rate. We present in fig. 10 the predicted integrated number counts for passive and active EROs (red dashed and blue dot-dashed lines respectively). In each panel, we also mark the surface densities corresponding to one detection in the *Herschel* Key Programmes<sup>1</sup> (GOODS-Herschel, HERMES, ATLAS, see caption for symbol coding). The result is not exciting: we predict that it is unlikely that these surveys will detect a large number of EROs. Incidentally, in the same figure we report our prediction for the integrated number counts of the whole galaxy population (thick solid line). Our differential number counts are in good agreement (dif-

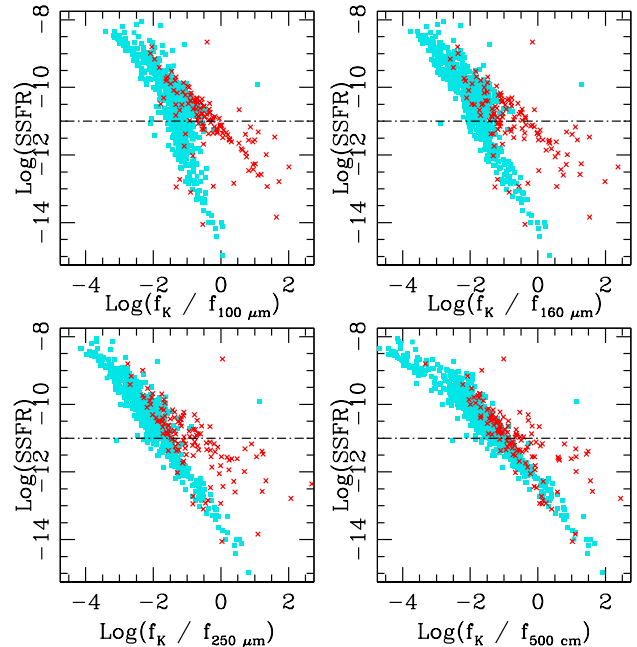


**Figure 9.** Predicted relation between the SSFR and the the ratio between the  $K$ -band and the monochromatic fluxes in four *Herschel* passbands, normalized to the  $K$ -band flux, for the EROs sample. Red crosses and cyan squares correspond to bulge- and disc- dominated model galaxies (splitted on the basis of their *bulge-to-total* ratio, with a threshold value of 0.6). Dot-dashed line represents the assumed threshold between active and passive EROs.

ference below 0.2 dex) with the results of Lacey et al. (2009) for infrared fluxes  $S > 1 \text{ mJy}$ ; at fainter fluxes MORGANA predicts a higher abundance of sources. It will be soon possible to compare this prediction with the forthcoming *Herschel* observations.

### 3.2 Evolutionary sequences in MORGANA.

In this section we focus on the relation between EROs (defined as objects with  $R - K > 5.0$  and  $K < 22$ ), sub-mm galaxies (defined as galaxies with a predicted  $850 \mu\text{m}$  flux  $f_{850\mu\text{m}} > 0.5 \text{ mJy}$ ) and local massive galaxies ( $M_* > 10^{11} M_\odot$  at  $z = 0$ ).

In order to use IR templates in place of the more expensive GRASIL, we define sub-mm bright galaxies as those objects with  $f_{850\mu\text{m}} > 0.5 \text{ mJy}$ , a flux where number counts based on the two methods are very similar (sec. 2.1) and only slightly higher than the limit reached in deep fields with currently available sub-mm telescopes.

For these three categories we follow their evolution in the redshift range  $0.5 < z < 4.5$ , with a time sampling of 100 Myr; for simplicity we restrict to the main progenitor branch of the galaxy merger tree. We check to what extent and in what time order a galaxy belonging to one category is observed as a member of another category.

As a first figure, the fraction of EROs that are seen *at the same time* as sub-mm sources is low, 0.1 per cent, while the fraction of sub-mm galaxies that are seen as (active) EROs is 5 per cent; then, the overlap between the two categories is rather small. In fig. 11 we show some diagnostics of the evolutionary path of galaxies in some specific category as a function of their galaxy stellar mass. The vertical arrows mark the mass limits within which the diagnostic

<sup>1</sup> <http://herschel.esac.esa.int/>

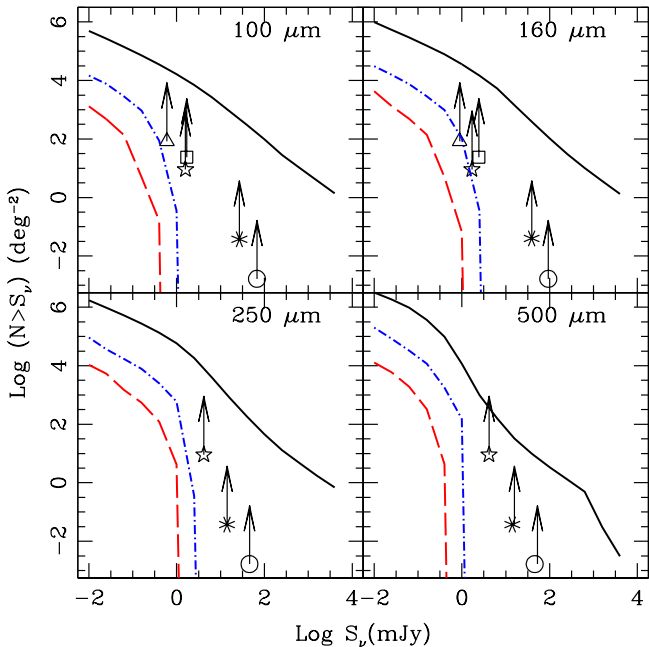


**Figure 10.** Predicted number counts in four *Herschel* passbands. The thick solid, red dashed and blue dot-dashed lines refer to the whole population, the passive and active EROs respectively. The symbols mark the surface density corresponding to the detection of one object in the GOODS-Herschel (triangle), PEP GOODS-S (square), HERMES Level-1 (star), Hermes Level-2 (asterisk) and ATLAS (circle) surveys

has sufficient statistics (only mass bins with at least 10 objects are considered). Panel (a) of Fig. 11 shows the fraction of EROs that are classified as sub-mm galaxy at an earlier epoch as a function of their stellar mass at the ERO epoch; the three histograms give this quantity for active, passive and all EROs (as specified in the legend). Almost all EROs with stellar masses  $\gtrsim 10^{11} M_{\odot}$  have had a sub-mm ancestor as a main progenitor, irrespective of their level of activity. The connection is soon lost at lower masses. In panel (b) of fig. 11 we select  $z > 1$  sub-mm sources and check whether they are predicted to be the main progenitors of a (passive or active or either) ERO. Here the stellar mass refers to the sub-mm selected galaxies. The resulting fraction is high and does not depend on stellar mass for  $M_{*} > 10^{9.75} M_{\odot}$ . This means that most sub-mm galaxies have an ERO descendant, which is in most cases an active ERO, while only roughly half of them have a passive ERO descendant.

We then consider the expected relation of the two high-redshift categories with local massive galaxies. Panel (c) of figure 11 shows the fraction of EROs and sub-mm galaxies that are *main* progenitors of a  $z = 0$  massive galaxy, as a function of their stellar mass at the observation redshift. More massive EROs and sub-mm galaxies are more likely to be main progenitors, and the relation is tighter for EROs, while sub-mm galaxies have a relatively modest,  $\sim 30$  per cent, probability. A different result is obtained when the main progenitors of local massive galaxies are considered, as in panel (d) of figure 11: here we report the fraction of local massive galaxies that have an ERO or sub-mm main progenitor, as a function of  $z = 0$  stellar mass (obviously larger than  $10^{11} M_{\odot}$ ). The main progenitor of a massive galaxy used to be an ERO more than 80 per cent of times and a sub-mm galaxy  $\sim 70$  per cent of times; as a matter of fact, each object may be seen as an ERO or sub-mm galaxy at many

redshifts. So, the low probabilities shown in panel (c) imply that many massive EROs or sub-mm galaxies end in massive galaxies not as main progenitors. In other words, consistently with the hierarchical clustering scenario, many massive galaxies will have not one but several ERO and/or sub-mm progenitors. However, panel (d) shows also that only  $\sim 20$  per cent of the main progenitors of local massive galaxies were both sub-mm galaxies and EROs (in this order) in their past.

The results in fig. 11 clearly depend on the adopted flux limit of sub-mm bright galaxies. Lowering (or raising) this flux has the effect of decreasing (increasing) the mass cutoff in panel (a), thus increasing (decreasing) the fraction of all EROs with sub-mm progenitors at intermediate masses. In panel (d), the fractions of sub-mm and ERO+sub-mm main progenitor increase (decrease) accordingly. Instead, the fractions shown in panels (b) and (c) are hardly affected as long as the flux limit is below 2 mJy.

In fig. 12 we consider the evolution of 5 representative model objects, chosen between the  $\sim 25$  per cent explicitly following the sub-mm – EROs – massive galaxy evolutionary sequence. In the four panels, from top to bottom, we show the total stellar mass (symbols mark the  $z = 0$  mass), the specific star formation rate, the  $R - K$  color and the  $850\mu\text{m}$  flux. The diversity of evolutionary tracks is evident from the figure, as well as the complexity of star formation histories. In most cases the two phases are well separated along the redshift evolution of the object. Some model galaxy undergoes repeated independent ERO (and sub-mm) episodes along their evolution; some of them can be seen both as an active and a passive ERO at different redshifts. Even if in most cases the ERO stage follows the sub-mm bright period, it is also possible that, as a result of late star formation activity, a model galaxy may be recognize as a sub-mm bright galaxy, even if it was a passive ERO at previous cosmic times. Interestingly, active EROs tend to have low sub-mm fluxes, consistently with the low fraction of galaxies that are at the same time ERO and sub-mm. These results show that the galaxy evolution sequences in our galaxy formation model based are more complex compared to the simple one obtained by Granato et al. (2004), that predict that massive galaxies go through sub-mm, quasar, ERO and passive phases.

## 4 CONCLUSIONS

In this paper we have discussed the statistical properties of the ERO population as predicted by the MORGANA galaxy formation model, in terms of number counts, redshift distributions and active fractions of  $R - K > 5$  sources. We generated mock photometric catalogues by interfacing MORGANA with the spectro-photometric + radiative transfer code GRASIL, and created large samples of model galaxies (so as to have good statistics on the rare EROs). We used both the *Padova* and the M05 SSP libraries; the latter include the contribution of TP-AGB stars. We combined the resulting UV-to-Near-IR synthetic SEDs, computed without the expensive Far-IR emission, with the Rieke et al. (2009) IR template library to estimate IR fluxes longward  $3\mu\text{m}$ . We then selected samples of EROs (and sub-mm galaxies) by applying the corresponding color and flux cuts.

We found that our standard model with *Padova* SSP library is able to reproduce the overall number counts and redshift distribution of the  $R - K > 5$  sources; the agreement worsens when redder cuts are considered. Other discrepancies, like the excess of faint EROs at deep  $K$  fluxes and the underestimate of the number of distant passive EROs, are consequences of well-known points of ten-

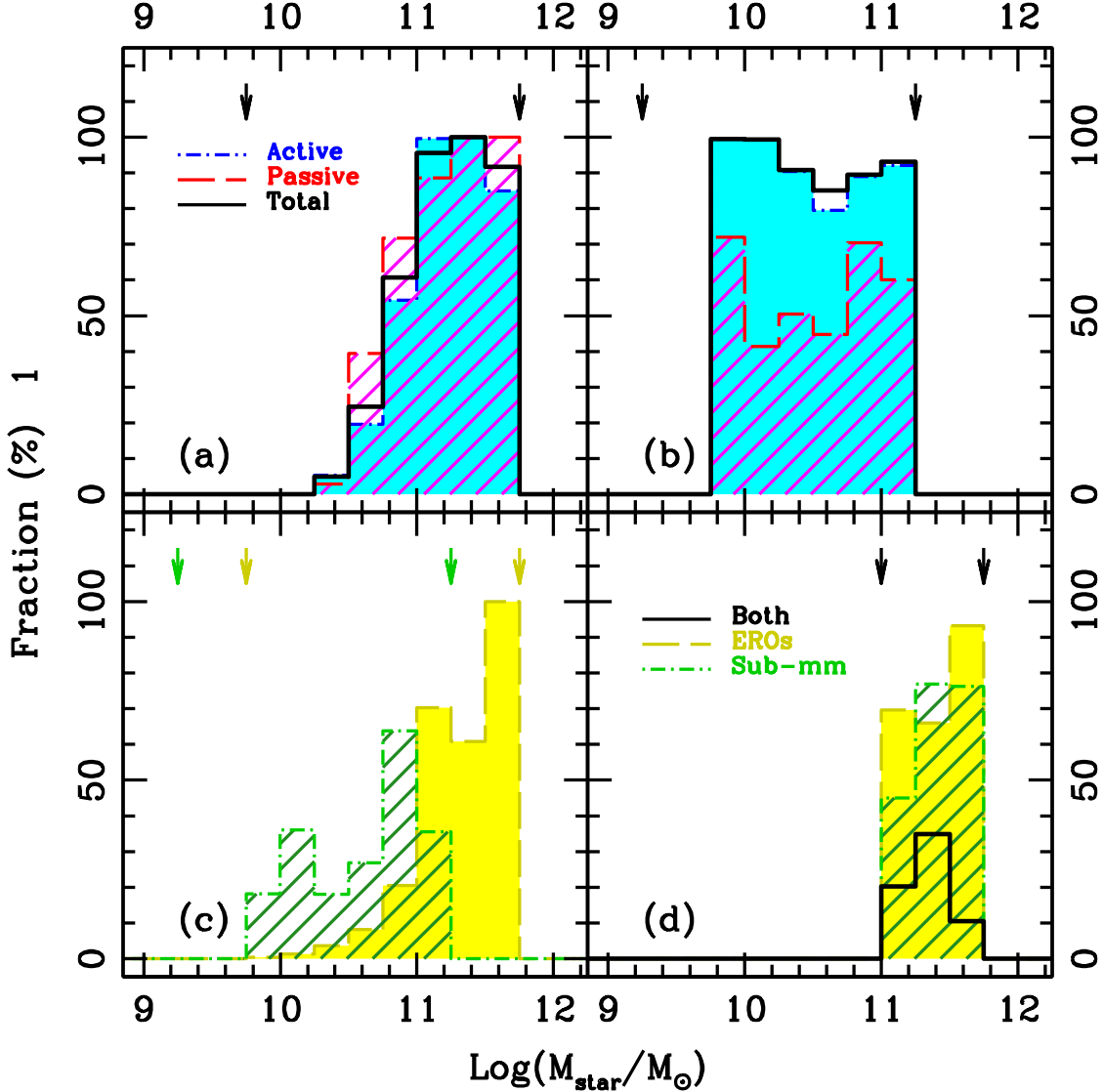


**Figure 11.** *Panel (a):* Fraction of EROs with a sub-mm main progenitor with  $f_{850\mu\text{m}} > 0.5$  mJy in MORGANA. Thick solid, red dashed (diagonal texture) and blue dot-dashed (cyan shading) histograms refer to the total and passive and active EROs respectively. *Panel (b):* Fraction of sub-mm galaxies that are the main progenitor of an ERO in MORGANA. Thick solid histogram refers to the total number of sub-mm galaxies, while the red dashed (diagonal texture) and blue dot-dashed (cyan shading) histograms indicate the properties of the descendant as indicated in the caption. *Panel (c):* Fraction of EROs (solid histogram and yellow shading) and sub-mm galaxies (green dot-dashed histogram and diagonal texture) that are main progenitors of a local massive galaxy ( $M_* > 10^{11} M_\odot$ ) as a function of their stellar mass. *Panel (d):* Fraction of massive ( $M_* > 10^{11} M_\odot$ ) galaxies at  $z < 0.2$  with a EROs (solid histogram yellow shaded area), a sub-mm progenitor ( $f_{850\mu\text{m}} > 0.5$  mJy green dot-dashed histogram and diagonal texture) or both (thick solid histogram). In all panels the vertical arrows indicate the mass limits for the reference sample of EROs, sub-mm and massive galaxies.

sion of the model with data, like the dearth of massive  $z > 2$  galaxies (Fontanot et al. 2007; Cirasuolo et al. 2008; Marchesini et al. 2009), or the excess of  $z \sim 1$  small galaxies (Fontanot et al. 2009b); this analysis does not reveal new discrepancies. Interestingly, MORGANA is able to roughly reproduce the substantial contribution (of the order of  $\sim 50\%$ , see e.g. Cimatti et al. 2002a; Miyazaki et al. 2003) of active galaxies to the global ERO population; here we define active galaxies as those with  $\text{SSFR} > 10^{-11}$  Gyr. We ascribe this success to the higher SSFR predicted by the model at higher redshifts (Fontanot et al. 2007; Santini et al. 2009).

We showed that the ERO number counts increase considerably when using the M05 SSP library. The addition of TB-AGBs gives a strong boost to the restframe SEDs of active galaxies long-

ward  $6000 \text{ \AA}$ , reddening them and thus increasing the number of active EROs. This leads to a good level of agreement even at very red cuts ( $R - K > 6$ ), though it does not completely solve the lack of very red passive galaxies at higher redshift. This highlights the importance of an accurate modeling of galactic synthetic SEDs when comparing the prediction of theoretical models of galaxy formation to observations, and confirms that TP-AGBs are a relevant ingredient for the correct reproduction of the high-redshift Universe (Maraston et al. 2006). The details of the modeling of dust attenuation also play a role: we checked that both increasing the fraction of cold gas locked into molecular clouds (as suggested by Lo Faro et al. 2009 to reproduce the properties of Lyman break Galaxies at  $z \gtrsim 4$ ) or using the analytical approach pro-



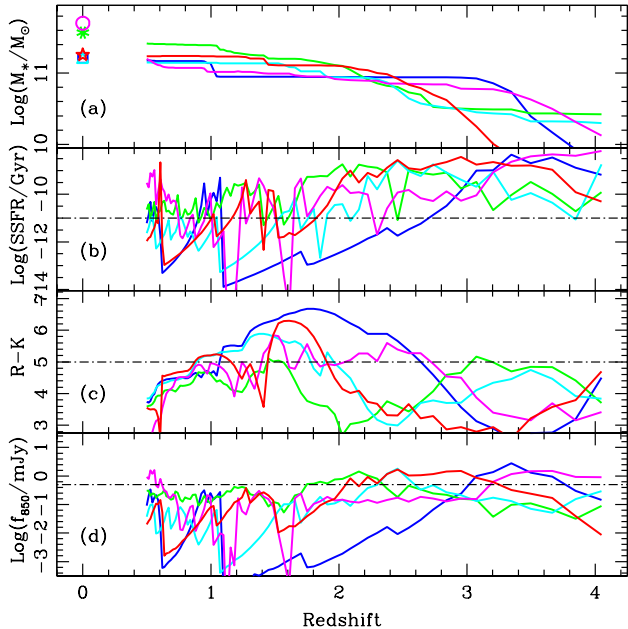


**Figure 12.** The redshift evolution of the total mass (panel a), SSFR (panel b), observer frame R-K color (Panel c), and observer frame  $850\mu\text{m}$  flux (Panel d) for 5 representative galaxies. In each panel the same greyscale corresponds to the same object. Empty symbols correspond to the  $z = 0$  mass of the 5 galaxies.

posed by De Lucia & Blaizot (2007) based on an universal attenuation law slightly reduces the number of active EROs ( $\lesssim 0.3$  dex at  $K \sim 20$ ).

We then considered the physical properties of the predicted ERO population with respect to a control sample of non color-selected galaxies with  $K < 22$  and  $1 < z < 2$ . Overall the physical properties of EROs do not differ significantly from those of a typical galaxy in the same redshift range, apart that active galaxies with low dust attenuation and low metallicities are excluded. We do not see any signature for a significant bimodality in the ERO population: the probability of a galaxy to be selected peaks in two regions of the  $\text{SSFR}-E(B-V)$  space, corresponding to moderately attenuated passive galaxies and strongly attenuated ( $E(B-V) > 0.2$ ) active galaxies, but this trend is not visible in the overall ERO distribution. This result is in agreement with Gonzalez-Perez et al. (2009). Deep fields in the Far-IR, from 100 to  $500\mu\text{m}$ , are the best way to constrain the SSFR of these objects, but presently planned surveys with *Herschel* will detect a small number of EROs at best.

We also tested the possible relation between EROs and both the sub-mm ( $f_{850\mu\text{m}} > 0.5$  mJy) galaxies and the local massive ( $M_* > 10^{11} M_\odot$ ) galaxies. This was done to test the suggestion that these different populations reflect well-defined stages of a typical evolutionary sequence of massive galaxies, like sub-mm galaxies evolving into EROs and later into massive passive galaxies. We found that most massive EROs have a sub-mm bright main progenitor and evolve into a massive galaxy at  $z = 0$ , and that many  $z = 0$  massive galaxies have an ERO or a sub-mm main progenitor, but only a minor fraction,  $\sim 25$  per cent, follow the sub-mm – ERO – massive galaxy sequence. Moreover, massive galaxies may easily have more than one sub-mm and/or ERO progenitor. In fact, star formation histories predicted by MORGANA are far more complex

and exhibit a great degree of diversity, with only a small sample following the well defined sequence described above.

Our work shows that EROs can be used as a powerful constraint for theories of galaxy formation and evolution, but a better and deeper understanding of the distribution of EROs in a configuration space defined by the physical quantities, like star formation activity, stellar mass, metallicity, stellar population ages and dust obscuration, is needed. Unfortunately, planned surveys with *Herschel* may not reach the combination of depth and area required for detecting and analysing statistically significant samples of EROs. On the other hand, the same instruments may provide the required spectroscopic and photometric follow-up in order to better understand the real nature of already detected EROs.

## ACKNOWLEDGMENTS

We thank Laura Silva for making the GRASIL code available and for many discussion; Claudia Maraston, Chiara Tonini and Bruno Henriquez for their help in including the M05 SSP library in our algorithm and for stimulant discussions; Gianluigi Granato, Lucia Pozzetti for useful comments. Some of the calculations were carried out on the PIA cluster of the Max-Planck-Institute für Astronomie at the Rechenzentrum Garching.

## REFERENCES

- Baugh C. M., 2006, Reports of Progress in Physics, 69, 3101  
 Bertelli G., Bressan A., Chiosi C., Fagotto F., Nasi E., 1994, A&AS, 106, 275  
 Bower R. G., Benson A. J., Malbon R., Helly J. C., Frenk C. S., Baugh C. M., Cole S., Lacey C. G., 2006, MNRAS, 370, 645  
 Brinchmann J., Charlot S., White S. D. M., Tremonti C., Kauffmann G., Heckman T., Brinkmann J., 2004, MNRAS, 351, 1151  
 Brown M. J. I., Jannuzi B. T., Dey A., Tiede G. P., 2005, ApJ, 621, 41  
 Caputi K. I., Dunlop J. S., McLure R. J., Roche N. D., 2004, MNRAS, 353, 30  
 Chabrier G., 2003, ApJ, 586, L133  
 Chapman S. C., Blain A. W., Smail I., Ivison R. J., 2005, ApJ, 622, 772  
 Charlot S., Fall S. M., 2000, ApJ, 539, 718  
 Cimatti A., Daddi E., Cassata P., Pignatelli E., Fasano G., Vernet J., Fomalont E., Kellermann K., Zamorani G., Mignoli M., Pozzetti L., Renzini A., di Serego Alighieri S., Franceschini A., Giallongo E., Fontana A., 2003, A&A, 412, L1  
 Cimatti A., Daddi E., Mignoli M., Pozzetti L., Renzini A., Zamorani G., Broadhurst T., Fontana A., Saracco P., Poli F., Cristiani S., D’Odorico S., Giallongo E., Gilmozzi R., Menci N., 2002a, A&A, 381, L68  
 Cimatti A., Mignoli M., Daddi E., Pozzetti L., Fontana A., Saracco P., Poli F., Renzini A., Zamorani G., Broadhurst T., Cristiani S., D’Odorico S., Giallongo E., Gilmozzi R., Menci N., 2002b, A&A, 392, 395  
 Cirasuolo M., McLure R. J., Dunlop J. S., Almaini O., Foucaud S., Simpson C., 2008, ArXiv e-prints, 804  
 Cirasuolo M., McLure R. J., Dunlop J. S., Almaini O., Foucaud S., Smail I., Sekiguchi K., Simpson C., Eales S., Dye S., Watson M. G., Page M. J., Hirst P., 2007, MNRAS, 380, 585  
 Cole S., Lacey C. G., Baugh C. M., Frenk C. S., 2000, MNRAS, 319, 168

- Cole S., Norberg P., Baugh C. M., Frenk C. S., Bland-Hawthorn J., Bridges T., Cannon R., Colless M. e. a., 2001, *MNRAS*, 326, 255
- Conselice C. J., Bundy K., U V., Eisenhardt P., Lotz J., Newman J., 2008, *MNRAS*, 383, 1366
- Daddi E., Cimatti A., Broadhurst T., Renzini A., Zamorani G., Mignoli M., Saracco P., Fontana A., Pozzetti L., Poli F., Cristiani S., D'Odorico S., Giallongo E., Gilmozzi R., Menci N., 2002, *A&A*, 384, L1
- Daddi E., Cimatti A., Renzini A., 2000, *A&A*, 362, L45
- De Lucia G., Blaizot J., 2007, *MNRAS*, 375, 2
- De Lucia G., Springel V., White S. D. M., Croton D., Kauffmann G., 2006, *MNRAS*, 366, 499
- Elston R., Rieke G. H., Rieke M. J., 1988, *ApJ*, 331, L77
- Firth A. E., Somerville R. S., McMahon R. G., Lahav O., Ellis R. S., Sabbey C. N., McCarthy P. J., Chen H., Marzke R. O., Wilson J., Abraham R. G., Beckett M. G., Carlberg R. G., Lewis J. R., Mackay C. D., Murphy D. C., Oemler A. E., Persson S. E., 2002, *MNRAS*, 332, 617
- Fontanot F., Monaco P., Cristiani S., Tozzi P., 2006, *MNRAS*, 373, 1173
- Fontanot F., Monaco P., Silva L., Grazian A., 2007, *MNRAS*, 382, 903
- Fontanot F., Somerville R. S., Silva L., 2010, in preparation, 1
- Fontanot F., Somerville R. S., Silva L., Monaco P., Skibba R., 2009a, *MNRAS*, 392, 553
- Fontanot F., De Lucia G., Monaco P., Somerville R. S., Santini P., 2009b, *MNRAS*, 397, 1776
- Gonzalez-Perez V., Baugh C. M., Lacey C. G., Almeida C., 2009, *MNRAS*, 398, 497
- Granato G. L., De Zotti G., Silva L., Bressan A., Danese L., 2004, *ApJ*, 600, 580
- Kang X., Jing Y. P., Silk J., 2006, *ApJ*, 648, 820
- Kimm T., Somerville R. S., Yi S. K., van den Bosch F. C., Salim S., Fontanot F., Monaco P., Mo H., Pasquali A., Rich R. M., Yang X., 2009, *MNRAS*, 394, 1131
- Komatsu E., Dunkley J., Nolte M. R., Bennett C. L., Gold B., Hinshaw G., Jarosik N., Larson D., Limon M., Page L., Spergel D. N., Halpern M., Hill R. S., Kogut A., Meyer S. S., Tucker G. S., Weiland J. L., Wollack E., Wright E. L., 2009, *ApJS*, 180, 330
- Kong X., Daddi E., Arimoto N., Renzini A., Broadhurst T., Cimatti A., Ikuta C., Ohta K., da Costa L., Olsen L. F., Onodera M., Tamura N., 2006, *ApJ*, 638, 72
- Kong X., Fang G., Arimoto N., Wang M., 2009, *ApJ*, 702, 1458
- Kroupa P., Tout C. A., Gilmore G., 1993, *MNRAS*, 262, 545
- Lacey C. G., Baugh C. M., Frenk C. S., Benson A. J., Orsi A., Silva L., Granato G. L., Bressan A., 2009, *ArXiv e-prints*
- Lagos C. D. P., Cora S. A., Padilla N. D., 2008, *MNRAS*, 388, 587
- Lawrence A., Warren S. J., Almaini O., Edge A. C., Hambly N. C., Jameson R. F., Lucas P., Casali M. e. a., 2007, *MNRAS*, 379, 1599
- Lo Faro B., Monaco P., Vanzella E., Fontanot F., Silva L., Cristiani S., 2009, *MNRAS*, 399, 827
- Maraston C., 2005, *MNRAS*, 362, 799
- Maraston C., Daddi E., Renzini A., Cimatti A., Dickinson M., Papovich C., Pasquali A., Pirzkal N., 2006, *ApJ*, 652, 85
- Marchesini D., van Dokkum P. G., Förster Schreiber N. M., Franx M., Labbé I., Wuyts S., 2009, *ApJ*, 701, 1765
- McCarthy P. J., Persson S. E., West S. C., 1992, *ApJ*, 386, 52
- Menci N., Fontana A., Giallongo E., Grazian A., Salimbeni S., 2006, *ApJ*, 647, 753
- Miyazaki M., Shimasaku K., Kodama T., Okamura S., Furusawa H., Ouchi M., Nakata F., Doi M. e. a., 2003, *PASJ*, 55, 1079
- Monaco P., Fontanot F., Taffoni G., 2007, *MNRAS*, 375, 1189
- Monaco P., Theuns T., Taffoni G., Governato F., Quinn T., Stadel J., 2002, *ApJ*, 564, 8
- Nagamine K., Cen R., Hernquist L., Ostriker J. P., Springel V., 2005, *ApJ*, 627, 608
- Pozzetti L., Mannucci F., 2000, *MNRAS*, 317, L17
- Rieke G. H., Alonso-Herrero A., Weiner B. J., Pérez-González P. G., Blaylock M., Donley J. L., Marcillac D., 2009, *ApJ*, 692, 556
- Roche N. D., Dunlop J., Almaini O., 2003, *MNRAS*, 346, 803
- Santini P., Fontana A., Grazian A., Salimbeni S., Fiore F., Fontanot F., Boutsia K., Castellano M., Cristiani S., de Santis C., Gallozzi S., Giallongo E., Menci N., Nonino M., Paris D., Pentericci L., Vanzella E., 2009, *A&A*, 504, 751
- Silva L., De Zotti G., Granato G. L., Maiolino R., Danese L., 2005, *MNRAS*, 357, 1295
- Silva L., Granato G. L., Bressan A., Danese L., 1998, *ApJ*, 509, 103
- Simpson C., Almaini O., Cirasuolo M., Dunlop J., Foucaud S., Hirst P., Ivison R., Page M., Rawlings S., Sekiguchi K., Smail I., Watson M., 2006, *MNRAS*, 373, L21
- Smail I., Owen F. N., Morrison G. E., Keel W. C., Ivison R. J., Ledlow M. J., 2002, *ApJ*, 581, 844
- Smith G. P., Smail I., Kneib J., Czoske O., Ebeling H., Edge A. C., Pelló R., Ivison R. J., Packham C., Le Borgne J., 2002, *MNRAS*, 330, 1
- Somerville R. S., Hopkins P. F., Cox T. J., Robertson B. E., Hernquist L., 2008, *MNRAS*, 391, 481
- Somerville R. S., Lee K., Ferguson H. C., Gardner J. P., Moustakas L. A., Giavalisco M., 2004, *ApJ*, 600, L171
- Stiavelli M., Treu T., 2001, in J. G. Funes & E. M. Corsini ed., *Galaxy Disks and Disk Galaxies Vol. 230 of Astronomical Society of the Pacific Conference Series, The Morphology of Extremely Red Objects*. pp 603–606
- Tonini C., Maraston C., Devriendt J., Thomas D., Silk J., 2009a, *MNRAS*, 396, L36
- Tonini C., Maraston C., Thomas D., Devriendt J., Silk J., 2009b, *ArXiv e-prints*
- Väisänen P., Johansson P. H., 2004, *A&A*, 421, 821
- Wang J., De Lucia G., Kitzbichler M. G., White S. D. M., 2008, *MNRAS*, 384, 1301
- Weinmann S. M., van den Bosch F. C., Yang X., Mo H. J., 2006, *MNRAS*, 366, 2